# A Spatially Distributed Multi-Period Optimal Power Flow Study with Distributed Battery Units

Aryan Ritwajeet Jha∗, *SIEEE*, Subho Paul†, *MIEEE*, Anamika Dubey∗, *SMIEEE*
∗*School of Electrical Engineering & Computer Science*, *Washington State University*, Pullman, WA, USA
†*Department of Electrical Engineering*, *Indian Institute of Technology (BHU) Varanasi*, Varanasi, UP, India
∗{aryan.jha, anamika.dubey}@wsu.edu, †{subho.eee}@iitbhu.ac.in

***Abstract*—The growing presence of battery-associated distributed energy resources (DERs) in distribution networks necessitates the development of multi-period optimal power flow (MPOPF) strategies. Generally, the MPOPF frameworks are developed as mixed integer non-convex programming (MINCP) and solved centrally. However, the main limitation of centralized MPOPF (MPCOPF) is its longer solution time, a typical solution time is in the order of $10^3$ to $10^4$ seconds. This article proposes a spatially distributed MPOPF (MPDOPF) to overcome such deficiencies. Initially, the OPF problem is developed as a single-phase MPCOPF for a distribution network consisting of distributed DERs and battery units. Later the original large-scale centralized OPF problem is split into multiple sub-problems, which are solved in parallel by sharing boundary voltage and power data with the neighboring agents by following the directives of the Equivalent Network Approximation method (ENApp). The performance characterization of the proposed MPDOPF framework is conducted using the IEEE 123 bus test system. This analysis offers insights into the superiority of distributed MPOPF frameworks over centralized ones concerning solution time.**

***Index Terms*—Batteries, distribution network, distributed energy resources (DERs), equivalent network approximation (ENApp)**

## I. Introduction

Presently, optimal power flow (OPF) tools are developed to run the MV/LV distribution grids in the most economical, reliable, and secure manner. The usefulness of OPF studies is gaining more interest due to the penetration of distributed energy resources (DERs), especially solar photovoltaic panels. Power generation from these DERs is influenced by the weather conditions, hence highly intermittent. Presently, deployment of battery units is becoming more pertinent to mitigate the uncertainty effect and maintain the power balance by controlling the charging and/or discharging operations [1]. However, the inclusion of batteries converts the conventional single-period time-decoupled OPF problem into a multi-period time-coupled OPF analysis.

Traditionally, centralized OPF (COPF) methods were popular where grid-edge data are accumulated at a central controller location [2]. The central controller is responsible for processing the accumulated data, solving the OPF algorithm, and dispatching control signals to the controlling resources. The centralized OPF algorithms are generally developed as a mixed integer non-convex programming (MINCP) problem and then simplified either as a convex problem by adopting second-order cone programming (SOCP) relaxations [3] [4], or as a linear problem by adopting Taylor series expansion [2], polyhedral approximations [5] or linear power flow models [6].

To overcome the scalability issues related to the COPF methods, distributed OPF (DOPF) algorithms are often proposed by decomposing the original COPF problem into multiple sub-problems, solved in parallel by permitting neighborhood communication. In this regard, the Auxiliary Problem Principle (APP) and the Alternating direction method of multipliers (ADMM) are two popular algorithms that are used to solve OPF problems as quadratic convex [7], SOCP relaxed convex [8], semidefinite programming (SDP) relaxed convex [9], [10], and linear programming problems [11]. Previously in [12], the authors' research group developed a DOPF framework based on the Equivalent Network Approximation method (ENApp) for solving DOPF problems with lesser macro iterations compared to ADMM.

The above references [3]- [11] mainly focused on developing single-time step OPF problems by neglecting the grid-edge devices having time-coupled operation, like batteries. The inclusion of battery models transforms a single-time step OPF into a multi-period OPF (MPOPF). Reference [13] propound a nonlinear multi-period centralized OPF (MPCOPF) framework to solve the active-reactive power dispatch from the batteries and DERs in a distribution network. Alizadeh and Capitanescu [14] proposed a stochastic security-constrained MPCOPF which is solved by sequentially solving a specific number of linear approximations of the original problem. Usman and Capitanescu [15] developed three different MPCOPF frameworks to solve stochastic AC OPF problems. All three approaches start by solving a linear program to fix the binary variables followed by either a linear or non-linear program to determine the continuous variables. Wu et al. [16] framed an MPOPF problem for a virtual power plant (VPP) collocated distribution network. The original centralized multi-parametric quadratic problem is decomposed into one master and multiple sub-problems for distribution network and VPPs, respectively by utilizing the concept of Benders Decomposition (BD). The sub-problems are solved in parallel and then the master problem is solved with the reported solutions of all the sub-problems.

It is evident from the above discussion that for the past few years several pieces of research have been conducted for developing MPOPF portfolios. However, the following

TABLE I: TAXONOMY TABLE FOR COMPARISON

| References | DERs | Batteries | Single period OPF | Multi-period OPF | Centralized OPF | Distributed OPF | Framework |
|---|---|---|---|---|---|---|---|
| [3], [4] | | | ✓ | | ✓ | | Convex |
| [5] | ✓ | | ✓ | | ✓ | | Linear |
| [6] | | | ✓ | | ✓ | | Linear |
| [7] | ✓ | | ✓ | | | ✓ | Convex (APP) |
| [8]- [10] | ✓ | | ✓ | | | ✓ | Convex (ADMM) |
| [11] | ✓ | | ✓ | | | ✓ | Linear (Accelerated ADMM) |
| [12] | ✓ | | ✓ | | | ✓ | Non-convex (ENApp) |
| [13] | ✓ | ✓ | | ✓ | ✓ | | Non-convex |
| [14], [15] | ✓ | ✓ | | ✓ | ✓ | | Linear/convex |
| [16] | ✓ | ✓ | | ✓ | | ✓ | Quadratic (BD) |
| This paper | ✓ | ✓ | | ✓ | | ✓ | Non-convex (ENApp) |

research gaps persist.

1) The MPOPF frameworks are mainly solved centrally [13]- [15]. The centralized methods suffer from scalability and computation challenges for bulk distribution grids and require longer solution time (in the range of a few thousand seconds).
2) Reference [16] proposed a distributed algorithm framework using BD. However, BD suffers from slow convergence and needs a central controller to solve the master problem.

This article aims to address the above research gaps by developing a spatially distributed MPOPF framework. The bulk distribution grid is divided into multiple networked areas, each solving its own local MPOPF problem and periodically communicating the values of boundary variables with neighboring areas. The interaction between the areas is modeled by following the principles of the ENApp distributed OPF algorithm. ENApp outperforms the other distributed algorithms

A taxonomy table to compare the existing studies and the present work is provided in I.

The specific contributions are as follows:

1) The overall problem is formulated as a non-convex programming and the

## II. Problem Formulation

### A. Notations

In this study, the distribution network is accounted as a tree (connected graph) having $N$ number of buses (indexed with $i$, $j$, and $k$) and the study is conducted for $T$ time steps (indexed by $t$), each of interval length $\Delta t$. The set of all such buses is $N$, and the sets of all buses with DERs and batteries are $D$ and $B$ respectively, such that $D, B \subseteq N$. A directed edge in the tree is represented by $(i, j)$ or $ij$ and the set containing all such edges is $\mathcal{L}$. Unless otherwise noted, $(i, j)$ indicates that bus $i$ is the 'upstream' or 'parent' bus of bus $j$, which itself may be considered as the 'downstream' or 'child' bus in relation. Each such line has resistance and reactance of $r_{ij}$ ohm and $x_{ij}$ ohm, respectively. Magnitude of the current flowing through the line at time $t$ is denoted by $I_{ij}^t$ $\left(l_{ij}^t = \left(I_{ij}^t\right)^2\right)$. The voltage magnitude of bus $j$ at time $t$ is given by $V_j^t$ $\left(v_j^t = \left(V_j^t\right)^2\right)$. Apparent power demand at a node $j$ at time $t$ is $s_{L_j}^t$ $(= p_{L_j}^t + jq_{L_j}^t)$. The uncontrolled active power generation from the DER present at bus $j$ at time step $t$ is denoted by $p_{D_j}^t$ and controlled reactive power dispatch from the DER inverter is $q_{D_j}^t$. Static capacitance attached to a node $j$ is denoted by $q_{C_j}$. The apparent power flow through line $ij$ at time step $t$ is $S_{ij}^t$ $(= P_{ij}^t + jQ_{ij}^t)$. In particular, the real power flowing from the substation into the network is denoted by $P_{Subs}^t$ and the associated cost involved per kW is $C^t$. The battery state of charge (soc) or energy level is $B_j^t$. Charging and discharging active power from battery inverter (of apparent power capacity $S_{R_j}^t$ ) are denoted by $P_{c_j}^t$ and $P_{d_j}^t$, respectively. The total state of charge capacity of the batteries are denoted by $B_{R_j}$, and the Rated battery powers are denoted by $P_{B_{R_j}}$. The reactive power support of the battery inverter is $q_{B_j}^t$. Rated apparent powers of DERs and Batteries at node $j$ are denoted by $S_{D_{R_j}}$ and $S_{B_{R_j}}$ respectively.

### B. Centralized Multi-Period OPF with Batteries

The OPF problem given in (1) aims to minimize the cost of power borrowed from the substation for the entire horizon. The incorporation of an additional 'Battery Loss' term ($\alpha > 0$) helps us bypass the usage of binary (integer) constraints for modelling the operation of batteries, which would otherwise make the optimization problem harder to solve. The term still ensures the complementarity of charging and discharging operations for any battery during a particular time period [17]–[19].

$$\min \sum_{t=1}^{T} \Bigg[ C^t P_{Subs}^t + \alpha \sum_{j \in \mathcal{B}} \Big\{ (1-\eta_C) P_{C_j}^t + \left(\frac{1}{\eta_D} - 1\right) P_{D_j}^t \Big\} \Bigg] \tag{1}$$

Subject to the constraints (2) to (13) given below:

$$0 = \sum_{(j,k)\in\mathcal{L}} \left\{P_{jk}^t\right\} - \left(P_{ij}^t - r_{ij} l_{ij}^t\right) - \left(P_{d_j}^t - P_{c_j}^t\right) - p_{D_j}^t + p_{L_j}^t \tag{2}$$

$$0 = \sum_{(j,k)\in\mathcal{L}} \left\{Q_{jk}^t\right\} - \left(Q_{ij}^t - x_{ij} l_{ij}^t\right) - q_{D_j}^t - q_{B_j}^t - q_{C_j} + q_{L_j}^t \tag{3}$$

$$0 = v_i^t - v_j^t - 2(r_{ij} P_{ij}^t + x_{ij} Q_{ij}^t) + \left\{r_{ij}^2 + x_{ij}^2\right\} l_{ij}^t \tag{4}$$

$$0 = (P_{ij}^t)^2 + (Q_{ij}^t)^2 - l_{ij}^t v_i^t \tag{5}$$

$$P_{Subs}^t \geq 0 \tag{6}$$

$$l_{ij}^t \in [0, I_{R,ij}^2] \tag{7}$$

$$v_j^t \in [V_{min}^2, V_{max}^2] \tag{8}$$

$$q_{D_j}^t \in \left[-\sqrt{{S_{D_{R,j}}}^2 - {p_{D_j}^t}^2}, \sqrt{{S_{D_{R,j}}}^2 - {p_{D_j}^t}^2}\right] \tag{9}$$

$$0 = B_j^t - \left\{B_j^{t-1} + \Delta t \eta_c P_{c_j}^t - \Delta t \frac{1}{\eta_d} P_{d_j}^t\right\} \tag{10}$$

$$P_{c_j}^t, P_{d_j}^t \in \left[0, P_{B_{R_j}}\right] \tag{11}$$

$$q_{B_j}^t \in [-0.44 P_{B_{R,j}}, 0.44 P_{B_{R,j}}] \tag{12}$$

$$B_j^t \in [soc_{min} B_{R,j}, soc_{max} B_{R,j}] \tag{13}$$

The distribution network is represented with the help of the branch power flow equations (2) to (5). Constraints (2) and (3) signify the active and reactive power balance at node $j$, including contributions from any attached DERs $(p_{D_j}^t, q_{D_j}^t, P_{c_j}^t, P_{d_j}^t, q_{B_j}^t)$ and/or batteries. The KVL equation for branch $(i,j)$ is represented by (4), while the equation describing the relationship between current magnitude, voltage magnitude and apparent power magnitude for nodes $i$ and $j$ is (5). Backflow of real power into the substation from the distribution system is avoided using the constraint (6).The box limits for squared branch current and squared node voltage are enforced via (7) and (8). (9) describes the reactive power limits of DER inverters. The trajectory of the state of charge of batteries versus time is given by (10) and is the only class of constraints in this paper coupling the optimal power flow problem in time. Battery charging and discharging powers are non-negative valued variables which should not exceed the battery's rated power capacity, as given by (11). Every battery's reactive power is also constrained based on the associated inverter's rated capacity, as described by (12). For safe and sustainable operation of the batteries, the state of charge $B_j^t$ is constrained to be within some percentage limits of the rated battery soc capacity, as given in (13)

### *C. ENApp based Distributed Multi-Period OPF with Batteries*

## III. Case Study Demonstration

### *A. Simulation Data: IEEE 123 Bus Test System*

We're using a Balanced Three-Phase version of the IEEE 123 Bus Test System, which has 85 Load Nodes. Additionally, 20% (17) and 30% (26) of these load nodes also contain reactive power controllable Solar photovolatics (PVs) and Batteries respectively. Their ratings are as per Table II. To demonstrate the effectiveness of the proposed algorithm, the Test System has been divided into four areas on similar lines as [12]. The full test system along with the area-wise division is shown in Figure 1.

It is assumed that a horizon-wide forecast for loads $p_L^t$, solar power output $p_D^t$ and cost of substation power $C^t$ is available to the distribution grid operator. Figure 2 shows the forecasted profiles for load, solar irradiance and cost of substation power over a 5 time-period horizon.

To showcase the workflow of the proposed algorithm, simulations were run for a 5 time-period horizon.

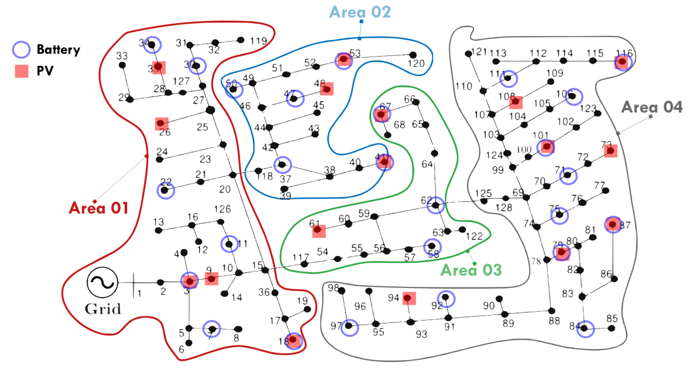


Fig. 1: IEEE 123 Node System Divided Into Four Areas

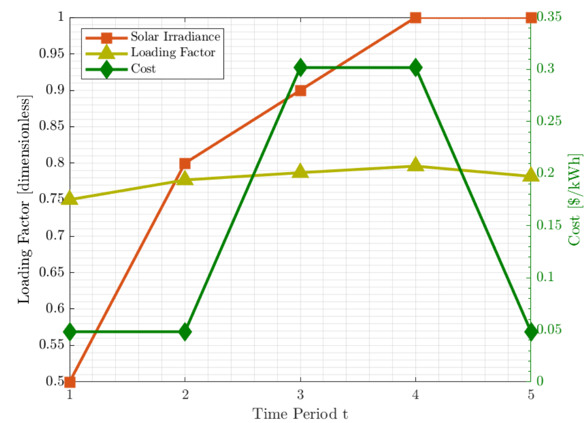


Fig. 2: Forecasts for Demand Power, Irradiance and Cost of Substation Power over a 5 Hour Horizon

TABLE II: Parameter Values

| Parameter | Value |
|---|---|
| $V_{min}, V_{max}$ | 0.95, 1.05 |
| $p_{D_{R_j}}$ | $0.33 p_{L_{R_j}}$ |
| $S_{D_{R_j}}$ | $1.2 p_{D_{R_j}}$ |
| $P_{B_{R_j}}$ | $0.33 p_{L_{R_j}}$ |
| $B_{R_j}$ | $T_{fullCharge} \times P_{B_{R_j}}$ |
| $T_{fullCharge}$ | 4 h |
| $\Delta t$ | 1 h |
| $\eta_C, \eta_D$ | 0.95, 0.95 |
| $soc_{min}, soc_{max}$ | 0.30, 0.95 |
| $\alpha$ | 0.001 |

### *B. Simulation Workflow*

All simulations were set up in MATLAB 2023a including both the high level algorithms as well as calls to the optimization solver. MATLAB's `fmincon` function was used to parse the nonlinear nonconvex optimization problem described by (1) to (13) in tandem with the SQP optimization algorithm to solve it. From the completed simulations, the resultant optimal control variables were obtained, and were passed through an OpenDSS engine (already configured with system data and forecast values) in order to check for the feasiblity of the results. The associated code may be found here.

In the following subsections, the proposed algorithm is compared against the centralized (MPCOPF) algorithm in terms of resultant optimal control variables, optimality gap in objective function and computational performance. Secondly, the resultant control variables are tested for ACOPF feasiblity against OpenDSS. Section III-C describes the comparison over a 5 time-period horizon with an additional focus on describing the workflow of the MPDOPF algorithm. Section III-D describes the comparsion over a 10 time-period horizon to test for the scalability of the MPDOPF algorithm.

### C. Simulation Results

The Test System

*1) Comparison between MPCOPF and MPDOPF:* In this section, comparative analyses are carried out between MPCOPF and MPDOPF considering 5-hour time steps.

TABLE III: Comparative analyses between MPCOPF and MPDOPF - 5 time-period horizon

| Metric | MPCOPF | MPDOPF |
|---|---|---|
| Biggest subproblem size | | |
| Decision variables | 3150 | 1320 |
| Linear constraints | 5831 | 2451 |
| Nonlinear constraints | 635 | 265 |
| Simulation results | | |
| Substation power cost ($) | 576.31 | 576.30 |
| Substation real power (kW) | 4308.28 | 4308.14 |
| Line loss (kW) | 75.99 | 76.12 |
| Substation reactive power (kVAR) | 574.18 | 656.24 |
| PV reactive power (kVAR) | 116.92 | 160.64 |
| Battery reactive power (kVAR) | 202.73 | 76.01 |
| Computation | | |
| Number of Iterations | - | 5 |
| Total Simulation Time (s) | 521.25 | 49.87 |

Further, here the

TABLE IV: ACOPF feasibility analyses - 5 time-period horizon

| Metric | MPDOPF | OpenDSS |
|---|---|---|
| Full horizon | | |
| Substation real power (kW) | 4308.14 | 4308.35 |
| Line loss (kW) | 76.12 | 76.09 |
| Substation reactive power (kVAR) | 656.24 | 652.49 |
| Max. all-time discrepancy | | |
| Voltage (pu) | 0.0002 | |
| Line loss (kW) | 0.0139 | |
| Substation power (kW) | 0.3431 | |

Boundary Variable Plots are too tall, make them slightly shorter, like 25% of the page only.

### D. Scalability Analysis

To demonstrate the effectiveness of the proposed algorithm over a bigger horizon to demonstrate scalability, simulations were run for a 10 time-period horizon. Figure 6 shows the forecasted profiles for load, solar irradiance and cost of substation power over the horizon.

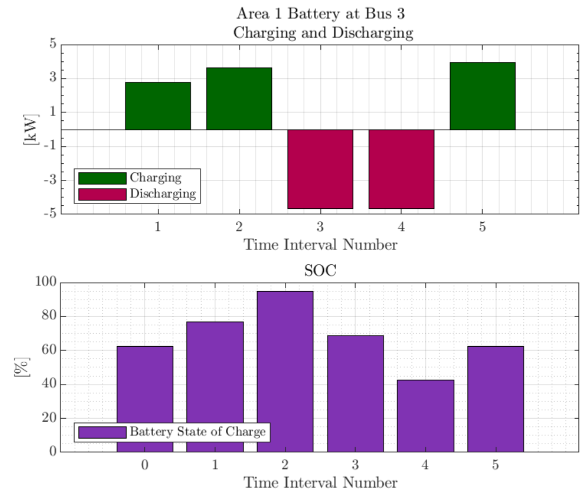


Fig. 3: Charging-Discharging and SOC graphs for Battery at Bus 3 located in Area 1 obtained by MPDOPF

TABLE V: Comparative analyses between MPCOPF and MPDOPF - 10 time-period horizon

| Metric | MPCOPF | MPDOPF |
|---|---|---|
| Biggest subproblem size | | |
| Decision variables | 6300 | 2640 |
| Linear constraints | 11636 | 4891 |
| Nonlinear constraints | 1270 | 530 |
| Simulation results | | |
| Substation power cost ($) | 1197.87 | 1197.87 |
| Substation real power (kW) | 8544.28 | 8544.04 |
| Line loss (kW) | 148.67 | 148.94 |
| Substation reactive power (kVAR) | 1092.39 | 1252.03 |
| PV reactive power (kVAR) | 222.59 | 139.81 |
| Battery reactive power (kVAR) | 388.52 | 310.94 |
| Computation | | |
| Number of Iterations | - | 5 |
| Total Simulation Time (s) | 4620.73 | 358.69 |

*1) Comparison between MPCOPF and MPDOPF:* In this section, comparative analyses are carried out between MPCOPF and MPDOPF considering 10-hour time steps with 20% PV penetration and 30% battery penetration.

Further, here the

TABLE VI: ACOPF feasibility analyses - 10 time-period horizon

| Metric | MPDOPF | OpenDSS |
|---|---|---|
| Full horizon | | |
| Substation real power (kW) | 8544.04 | 8544.40 |
| Line loss (kW) | 148.94 | 148.87 |
| Substation reactive power (kVAR) | 1252.03 | 1243.36 |
| Max. all-time discrepancy | | |
| Voltage (pu) | 0.0002 | |
| Line loss (kW) | 0.0132 | |
| Substation power (kW) | 0.4002 | |

## IV. Conclusions

[17], [18], [20]–[22]

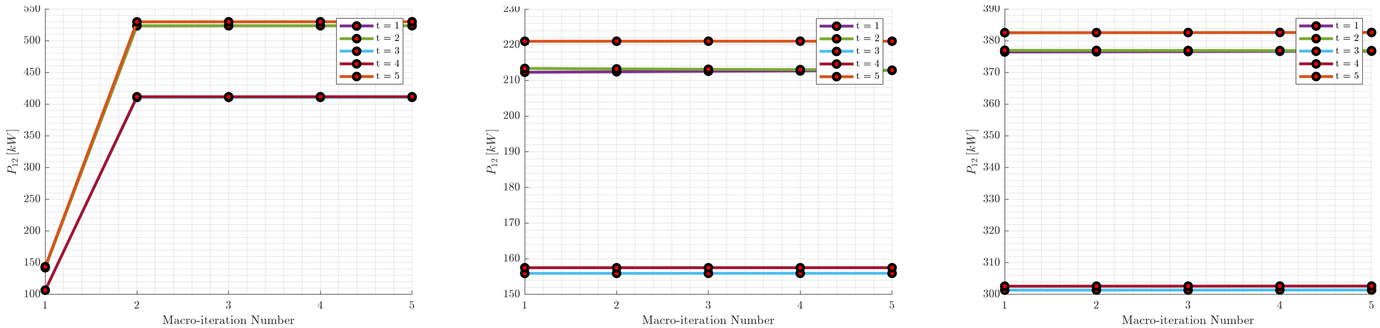


(a) Real Power flowing from Area 1 into Area 2 (b) Real Power flowing from Area 1 into Area 3 (c) Real Power flowing from Area 2 into Area 4

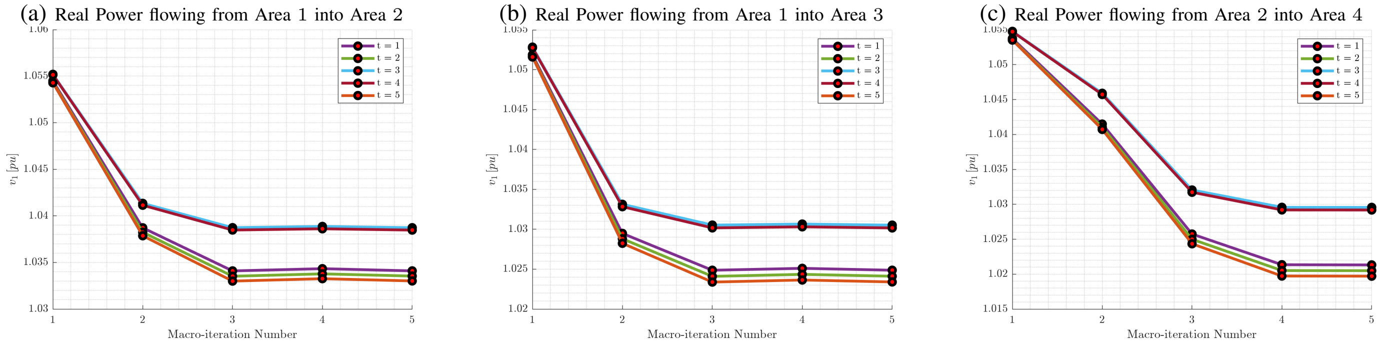


(d) Voltage at the PoI of Area 1 and Area 2 (e) Voltage at the PoI of Area 1 and Area 3 (f) Voltage at the PoI of Area 2 and Area 4

Fig. 4: Convergence of Boundary variables with every iteration. Each plot represents a particular variable exchanged between a pair of connected areas. Each line graph within a plot represents a particular time period.

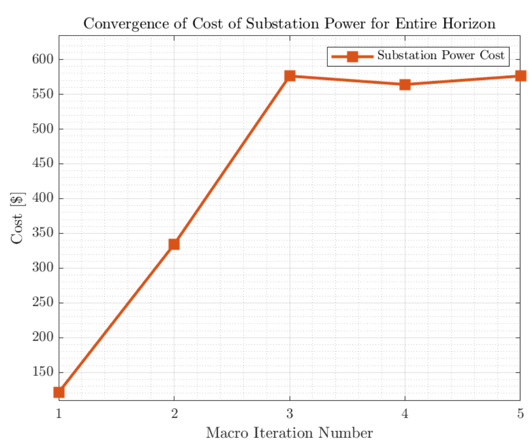


Fig. 5: Convergence of Objective Function Value with each MPDOPF iteration

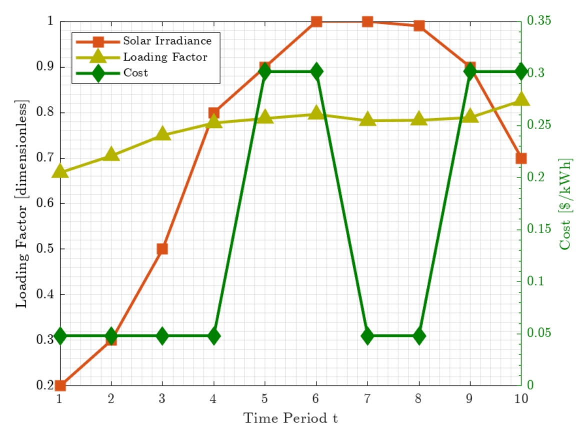


Fig. 6: Forecasts for Demand Power, Irradiance and Cost of Substation Power over a 10 Hour Horizon

## REFERENCES


[1] T. Gangwar, N. P. Padhy, and P. Jena, "Storage allocation in active distribution networks considering life cycle and uncertainty," IEEE Trans. Ind. Inform., vol. 19, no. 1, pp. 339–350, Jan. 2023.

[2] S. Paul and N. P. Padhy, "Real-time advanced energy-efficient management of an active radial distribution network," IEEE Syst. J., vol. 16, no. 3, pp. 3602–3612, Sept. 2022.

[3] W. Wei, J. Wang, and L. Wu, "Distribution optimal power flow with real-time price elasticity," IEEE Trans. Power Syst., vol. 33, no. 1, pp. 1097–1098, Jan. 2018.

[4] M. M.-U.-T. Chowdhury, B. D. Biswas, and S. Kamalasadan, "Second-order cone programming (socp) model for three phase optimal power flow (opf) in active distribution networks," IEEE Trans. Smart Grid, vol. 14, no. 5, pp. 3732–3743, 2023.

[5] Z. Guo, W. Wei, L. Chen, Z. Dong, and S. Mei, "Parametric distribution optimal power flow with variable renewable generation," IEEE Trans. Power Syst., vol. 37, no. 3, pp. 1831–1841, May 2022.

[6] H. Yuan, F. Li, Y. Wei, and J. Zhu, "Novel linearized power flow and linearized opf models for active distribution networks with application in distribution lmp," IEEE Trans. Smart Grid, vol. 9, no. 1, pp. 438–448, Jan. 2018.

[7] A. R. Di Fazio, C. Risi, M. Russo, and M. De Santis, "Decentralized voltage optimization based on the auxiliary problem principle in distribution networks with ders," Appl. Sci., vol. 11, no. 4509, pp. 1–24, 2021.

[8] W. Zheng, W. Wu, B. Zhang, H. Sun, and Y. Liu, "A fully distributed

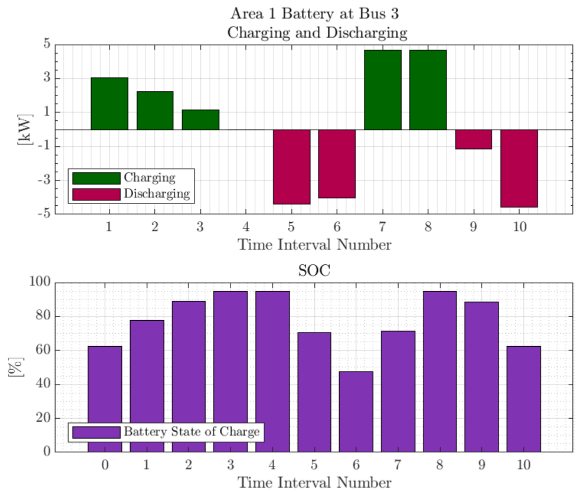


Fig. 7: Charging-Discharging and SOC graphs for Battery at Bus 3 located in Area 1 obtained via MPDOPF


reactive power optimization and control method for active distribution networks," IEEE Trans. Smart Grid, vol. 7, no. 2, pp. 1021–1033, Mar. 2016.

[9] P. Wang, Q. Wu, S. Huang, C. Li, and B. Zhou, "Admm-based distributed active and reactive power control for regional ac power grid with wind farms," J. Modern Power Syst. Clean Energy, vol. 10, no. 3, pp. 588–596, May 2022.

[10] B. D. Biswas, M. S. Hasan, and S. Kamalasadan, "Decentralized distributed convex optimal power flow model for power distribution system based on alternating direction method of multipliers," IEEE Trans. Ind. Appl., vol. 59, no. 1, pp. 627–640, Jan.-Feb. 2023.

[11] S. Paul, B. Ganguly, and S. Chatterjee, "Nesterov-type accelerated admm (n-admm) with adaptive penalty for three-phase distributed opf under non-ideal data transfer scenarios," in 2023 IEEE 3rd International Conference on Smart Technologies for Power, Energy and Control (STPEC), 2023, pp. 1–6.

[12] R. Sadnan and A. Dubey, "Distributed optimization using reduced network equivalents for radial power distribution systems," IEEE Trans. Power Syst., vol. 36, no. 4, pp. 3645–3656, Jul. 2021.

[13] A. Gabash and P. Li, "Active-reactive optimal power flow in distribution networks with embedded generation and battery storage," IEEE Trans. Power Syst., vol. 27, no. 4, pp. 2026–2035, Nov. 2012.

[14] M. I. Alizadeh and F. Capitanescu, "A tractable linearization-based approximated solution methodology to stochastic multi-period ac security-constrained optimal power flow," IEEE Trans. Power Syst., vol. 38, no. 6, pp. 5896–5908, 2023.

[15] M. Usman and F. Capitanescu, "Three solution approaches to stochastic multi-period ac optimal power flow in active distribution systems," IEEE Trans. Sustain. Energy, vol. 14, no. 1, pp. 178–192, 2023.

[16] C. Wu, W. Gu, S. Zhou, and X. Chen, "Coordinated optimal power flow for integrated active distribution network and virtual power plants using decentralized algorithm," IEEE Trans. Power Syst., vol. 36, no. 4, pp. 3541–3551, Jul. 2021.

[17] N. Nazir and M. Almassalkhi, "Receding-Horizon Optimization of Unbalanced Distribution Systems with Time-Scale Separation for Discrete and Continuous Control Devices," pp. 1–7, Jun. 2018.

[18] N. Nazir, P. Racherla, and M. Almassalkhi, "Optimal multi-period dispatch of distributed energy resources in unbalanced distribution feeders," Jun. 2019.

[19] N. Nazir and M. Almassalkhi, "Guaranteeing a Physically Realizable Battery Dispatch Without Charge-Discharge Complementarity Constraints," IEEE Trans. Smart Grid, vol. 14, no. 3, pp. 2473–2476, Sep. 2021.

[20] M. Farivar and S. H. Low, "Branch flow model: Relaxations and convexification," 2012 IEEE 51st IEEE Conference on Decision and Control (CDC), pp. 3672–3679, Dec. 2012.

[21] A. Agarwal and L. Pileggi, "Large Scale Multi-Period Optimal Power Flow With Energy Storage Systems Using Differential Dynamic Programming," pp. 1750–1759, Sep. 2021.

[22] X. Qian and Y. Zhu, "Differential Dynamic Programming for Multistage Uncertain Optimal Control," pp. 88–92, Jul. 2014.